Inorganic Chemistry
Article

Inorg. Chem. **2010**, *49*, 2083–2092 **2083**
DOI: 10.1021/ic901849e

Formation of a Cobalt(III)−Phenoxyl Radical Complex by Acetic Acid Promoted Aerobic Oxidation of a Co(II)salen Complex

Evi Vinck,[†] Damien M. Murphy,[‡] Ian A. Fallis,[‡] Robert R. Strevens,[‡] and Sabine Van Doorslaer*[,†]

[†]*Department of Physics, University of Antwerp, B-2610 Antwerp, Belgium, and* [‡]*School of Chemistry, Cardiff University, Main Building, Park Place, Cardiff CF10 3TB, United Kingdom*

Received September 18, 2009

The activation of *N,N′*-bis(3,5-di-*tert*-butylsalicylidene)-1,2-cyclohexane-diamino Co^{II}, [Co^{II}(**1**)], by the addition of acetic acid under aerobic conditions has been investigated by a range of spectroscopic techniques including continuous-wave EPR, HYSCORE, pulsed ENDOR, and resonance Raman. These measurements have revealed for the first time the formation of a coordinated cobalt(III)-bound phenoxyl radical labeled [Co^{III}(**1**$^{\bullet}$)$(OAc)_n$]$(OAc)_m$ ($n = m = 1$ or $n = 2$, $m = 0$). This cobalt(III)-bound phenoxyl radical is characterized by the following spin Hamiltonian parameters: $g_x = 2.0060$, $g_y = 2.0031$, $g_z = 1.9943$, A_x = 17 MHz, A_y = 55 MHz, and A_z = 14 MHz. Although the radical contains coordinated acetate(s), the experiments unambiguously proved that the phenoxyl radical is situated on ligand (**1**) as opposed to a phenoxyl radical ligated to cobalt in the axial position. Density functional theory computations on different models corroborate the stability of such a phenoxyl radical species and suggest the ligation of one or two acetate molecules to the complex. A mechanism is proposed, which accounts for the formation of this unusual and extremely robust phenoxyl radical, never previously observed for [Co(**1**)].

Introduction

Metal-bound phenoxyl radicals have been extensively studied, mainly due to the discovery of a Cu^{II}-tyrosyl radical in the active site of galactose oxidase (GOase) and glyoxal oxidase.[1,2] Owing to the central role of the metal atom coupled to a phenoxyl radical (i.e., an inorganic and organic cofactor) in performing biological oxidation reactions, several synthetic approaches have been developed to mimic this activity.[3−5] In many cases, metal phenolate macrocyclic complexes or tetradentate Schiff base complexes, with bulky substituents, were found to lead to species described either as a metal−ligand radical ($M^{n+}(L^{\bullet})$) or as a high valent metal complex ($M^{(n+1)+}(L^{-})$) after undergoing a one electron oxidation by electrochemical means.[6,7] These phenolate−transition-metal complexes can be one-electron oxidized to generate the corresponding stable phenoxyl radical complex, provided the phenolate is suitably protected by bulky substituents in the *ortho*- and *para*- positions (such as *tert*-butyl groups). Quite often, the localization of the oxidation site can be metal centered or ligand centered:[6,7]

$$M^{n+}-O-R \; -1e^{-} \rightarrow M^{n+}-O^{\bullet}-R \text{ or } M^{(n+1)+}-O-R \quad (1)$$

Although most oxidized metal−phenolate complexes have only one characteristic oxidation state (i.e., a metal-phenoxyl radical state or a high valent metal phenolate, as in eq 1), temperature dependent tautomerism between the two states has been reported.

In this work, we report the acid-mediated formation of a $cobalt^{III}$ bound phenoxyl radical during the activation process of a well-known catalyst, i.e., the *N,N′*-bis(3,5-di-*tert*-butylsalicylidene)-1,2-cyclohexane-diamino Co^{II} salen complex, [Co(**1**)] (Scheme 1). The catalyst is activated by the addition of acetic acid under air to [Co(**1**)].[8] The resulting complex is widely used to separate the enantiomers in racemic mixtures of terminal epoxides via a hydrolytic kinetic resolution (HKR) reaction. Despite its widespread use, the activated catalyst is poorly characterized. Previous studies revealed that the activated form certainly contains Co^{III}; however, there appears to be some contradictory reports on the diamagnetic versus paramagnetic nature of the activated complex.[9−11] In a recent NMR study of the activated

*To whom correspondence should be addressed. Fax: +32/3/265 24 70. E-mail: sabine.vandoorslaer@ua.ac.be.

(1) Borman, C. D.; Saysell, C. G.; Sokolowski, A.; Twitchett, M. B.; Wright, C.; Sykes, A. G. *Coord. Chem. Rev.* **1999**, *192*, 771–779.
(2) Whittaker, M. M.; Whittaker, J. W. *J. Biol. Chem.* **1988**, *263*, 6074–6080.
(3) Chaudhuri, P.; Wieghardt, K. *Prog. Inorg. Chem.* **2001**, *50*, 151–216.
(4) Jazdzewski, B. A.; Tolman, W. B. *Coord. Chem. Rev.* **2000**, *200*, 633–685.
(5) Ray, K.; Petrenko, T.; Wieghardt, K.; Neese, F. *Dalton. Trans.* **2007**, 1552–1566.
(6) Pratt, R. C.; Stack, T. D. P. *J. Am. Chem. Soc.* **2003**, *125*, 8716–8717.
(7) Storr, T.; Wasinger, E. C.; Pratt, R. C.; Stack, T. D. P. *Angew. Chem., Int. Ed.* **2007**, *46*, 5198–5201.
(8) Kim, G. J.; Lee, H.; Kim, S. J. *Tetrahedron Lett.* **2003**, *44*, 5005–5008.
(9) White, D. E.; Jacobsen, E. N. *Tetrahedron: Asymmetry* **2003**, *14*, 3633–3638.
(10) Furrow, M. E.; Schaus, S. E.; Jacobsen, E. N. *J. Org. Chem.* **1998**, *63*, 6776–6777.
(11) Kemper, S.; Hrobarik, P.; Kaupp, M.; Schlorer, N. E. *J. Am. Chem. Soc.* **2009**, *131*, 4172.

Published on Web 02/02/2010

Scheme 1. The Structure of (*R*,*R*)-*N*,*N*′-bis(3,5-di-*tert*-butylsalicylidene)-1,2-cyclohexane-diamino Co^{II} (hereafter labeled (*R*,*R*)-[Co(**1**)]) and Proposed Structures of Species A ($[Co^{III}(\mathbf{1}^{\bullet})(OAc)_2]$) and Species B ($[Co^{III}(\mathbf{1}^{\bullet})(Py)_2]^{2+}$)

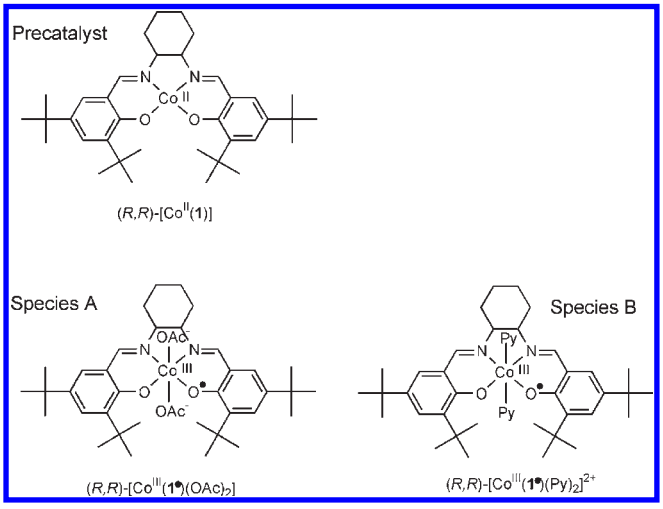

catalyst,[11] a paramagnetic pentacoordinated high-spin species was observed.

The spectroscopic measurements described here unambiguously reveal the presence of a stable coordinated (paramagnetic) phenoxyl radical in the activated system. This phenoxyl radical species will be analyzed in detail using a combination of continuous-wave and pulsed electron paramagnetic resonance (EPR) and resonance Raman (RR) techniques. Furthermore, the characteristics of the radical will be further investigated using density-functional-theory (DFT) computations, which will be compared in detail with the experimental results.

Experimental Section

Sample Preparation. (*R*,*R*)-[Co(1)]. (*R*,*R*)-*N*,*N*′-bis(3,5-di-*tert*-butylsalicylidene)-1,2-cyclohexane-diamino cobalt^{II} was prepared and purified from (*R*,*R*)-H_2**1**[12] by the method of Leung et al.[13] This enantiomer of the complex was used throughout this study. For the EPR analyses, the complex was dissolved in toluene. Concentrations of 80 mM were used for the CW- and pulsed-EPR experiments and ~0.1 mM for the RR measurements.

To obtain acid-activated complexes, 10 equiv of acetic acid was added to a toluene solution of (*R*,*R*)-[Co(**1**)] (80 mM) under air. For some experiments, ^{13}C-labeled acetic acid (acetic acid-1-^{13}C, Sigma Aldrich, 99 atom %^{13}C) was used.

In order to test the ability of axial ligand binding to the different complexes, pyridine (Fluka, puriss.) was sometimes added (see the Results for a detailed description).

Spectroscopic Techniques. The X-band CW-EPR experiments were performed on a Bruker ESP300E spectrometer (microwave (mw) frequency 9.45 GHz) equipped with a gas-flow cryogenic system (Oxford, Inc.), allowing operation from room temperature down to 2.5 K. The magnetic field was measured with a Bruker ER035 M NMR Gaussmeter. The spectra were recorded at a temperature of 100 K, using a microwave power of 2 mW, a modulation amplitude of 0.2 mT, and a modulation frequency of 100 kHz.

The W-band CW-EPR experiments were performed on an Elexsys Bruker spectrometer E680 (mw frequency 94 GHz), equipped with a continuous flow cryostat and a super conductive magnet from Oxford, Inc. The measurements were done at 100 K, using a microwave power of 0.044 mW, a modulation amplitude of 0.5 mT, and a modulation frequency of 100 kHz. Simulations of all CW-EPR spectra were performed with the EasySpin program, a Matlab toolbox developed for EPR simulations[14] (www.easyspin.org).

The X-band pulsed EPR and pulsed ENDOR experiments were performed with an ESP380E Bruker spectrometer (mw frequency 9.76 GHz) equipped with a liquid-helium cryostat from Oxford Inc. All experiments were done at different temperatures from 4 to 30 K (see details in the figure captions) and a repetition rate of 1 kHz. The magnetic field was measured with a Bruker ER035 M NMR Gaussmeter.

Hyperfine sublevel correlation (HYSCORE) experiments[15] were carried out using the pulse sequence $\pi/2-\tau-\pi/2-t_1-\pi-t_2-\pi/2-\tau-$echo, with pulse lengths of $t_{\pi/2} = t_{\pi} = 16$ ns. Times t_1 and t_2 were varied from 96 to 5680 ns in steps of 16 ns. An eight-step phase cycle was used to eliminate unwanted echoes. The individual time traces were baseline corrected with a third-order polynomial, apodized with a Hamming window, and zero-filled. After 2D Fourier transformation, the absolute-value spectrum was calculated. The HYSCORE spectra were simulated using a GAMMA-based[16] program developed at the ETH Zurich.[17] The same sets of τ values as in the experiments were taken. For the simulation, ideal pulses were used with the same interpulse distances as in the experiment. The Euler angles α, β, and γ define an active rotation (right-hand) of the matrices and tensors with respect to the *g* principal axes system (i.e., rotation about the *z* axis over angle α, followed by rotation of angle β about the new *y* axis, with subsequent rotation about the new *z* axis over angle γ). In order to optimize the proton or ^{13}C signal intensity, the second and third $\pi/2$ pulses were replaced by matched pulses of 40 or 48 ns (protons) and 64 ns (^{13}C) in length, with strength $\nu_1 = 15.625$ MHz (protons) and 3.91 MHz (^{13}C).[18]

The Mims-ENDOR experiments[19] were performed using the pulse sequence $\pi/2-\tau-\pi/2-T-\pi/2-\tau-$echo, with mw pulse lengths of $t_{\pi/2} = 16$ ns and interpulse times varied from $\tau = 96$ to 1696 ns. During time *T* (13.8 μs), an rf pulse with variable frequency and a length of 11 μs was applied. Davies-ENDOR experiments[20] were carried out using the following pulse sequence: $\pi-T-\pi/2-\tau-\pi-\tau-$echo. The experiments were done with mw pulse lengths of $t_{\pi} = 48$ ns and $t_{\pi/2} = 24$ ns and an interpulse time τ of 176 ns. An rf π pulse of variable frequency and a length of 5.4 μs was applied during time *T*.

Resonance Raman (RR) measurements were carried out on an 80 cm Dilor XY-800 Raman scattering spectrometer consisting of a triple spectrograph, operating in the normal mode, and a liquid-nitrogen cooled CCD detector. The excitation source was a Kr-ion laser (Spectra Physics 2020) at 413.1 nm. Five spectra (200 s recording time) were acquired and averaged after the removal of cosmic ray spikes by an in-house developed program. Laser powers of 10 mW were used.

DFT Computations. Spin-unrestricted density functional computations were performed with the ORCA package[21−25]

(12) Larrow, J. F.; Jacobsen, E. N. *Org. Synth.* **1998**, *75*, 1–11.
(13) Leung, W. H.; Chan, E. Y. Y.; Chow, E. K. F.; Williams, I. D.; Peng, S. M. *J. Chem. Soc., Dalton Trans.* **1996**, 1229–1236.
(14) Stoll, S.; Schweiger, A. *J. Magn. Reson.* **2006**, *178*, 42–55.
(15) Höfer, P.; Grupp, A.; Nebenführ, H.; Mehring, M. *Chem. Phys. Lett.* **1986**, *132*, 279–282.
(16) Smith, S. A.; Levante, T. O.; Meier, B. H.; Ernst, R. R. *J. Magn. Reson.* **1994**, *106*, 75–105.
(17) Madi, Z. L.; Van Doorslaer, S.; Schweiger, A. *J. Magn. Reson.* **2002**, *154*, 181–191.
(18) Jeschke, G.; Rakhmatullin, R.; Schweiger, A. *J. Magn. Reson.* **1998**, *131*, 261–271.
(19) Mims, W. B. *Proc. R. Soc. A, Math. Phys. Eng. Sci.* **1965**, *283*, 452–457.
(20) Davies, E. R. *Phys. Lett. A* **1974**, *A 47*, 1–2.
(21) Neese, F. *J. Chem. Phys.* **2001**, *115*, 11080–11096.
(22) Neese, F. *J. Phys. Chem. A* **2001**, *105*, 4290–4299.
(23) Neese, F. *J. Chem. Phys.* **2003**, *118*, 3939–3948.
(24) Neese, F. *J. Chem. Phys.* **2005**, *122*, 34107.
(25) Ray, K.; Begum, A.; Weyhermuller, T.; Piligkos, S.; van Slageren, J.; Neese, F.; Wieghardt, K. *J. Am. Chem. Soc.* **2005**, *127*, 4403–4415.

on different [Co(**1**)]-derived complexes modeling the acid activation. Geometry optimization was performed with the B3LYP functional, with an Ahldrich-TZV basis set[26] with pp polarization functions (TZVPP) [Ahldrich and co-workers, unpublished] for the cobalt ion, and Gaussian 6_31G basis functions[27,28] with polarization functions from the basis 6-311++G(d,p)[29] for the other atoms. For the calculation of the hyperfine principal values, basis sets with more flexibility in the core region were tried, i.e., the ORCA basis sets "CoreProp" (CP) for the cobalt ion and "EPRII" or "EPRIII"[30] for the nitrogens, protons, or carbons. The basis sets are mentioned in the figure/table captions.

In order to account for solvent effects, some calculations were performed with the conductor-like screening model (COSMO) that is implemented in ORCA.[31] The dielectric constant of the toluene (ε_1 = 2.4 at 20 °C)/acetic acid (ε_2 = 6.2 at 20 °C) mixture was calculated using the formulas given in ref 32, yielding a constant of 2.5.

The calculations, including solvent effects, gave very similar results as the *in vacuo* calculations and are not shown throughout the paper.

Results

Acid Activation of (*R*,*R*)-[Co(1)]. In our previous work,[33] the precatalyst complex (*R*,*R*)-[Co(**1**)] (Scheme 1) was shown to have electronic properties characteristic of a low-spin (LS) Co^{II} Schiff-base complex. The X-band EPR spectrum of this parent complex is shown in Figure 1a as a reference and is typical for a species with $|yz, {}^2A_2>$ ground state[34] (g_x = 3.21, g_y = 1.89, g_z = 1.98; $A_x = \pm 400$ MHz, $|A_y| < 80$ MHz, $A_z = \pm 125$ MHz). As mentioned in the Introduction, activation of this precatalyst complex for the HKR application is achieved by the addition of a weak organic acid, such as acetic acid, while stirring constantly under air (for ~30 min).

Upon the addition of acetic acid to [Co(**1**)] under aerobic conditions, the EPR spectrum in Figure 1a disappears completely and is replaced by a series of complex and overlapping EPR signals stemming from different paramagnetic species (data not shown); these signals are only observed at low temperatures (2.5 K). However, at higher temperatures (100 K), a weak paramagnetic species, which accounts for 1−2% of the original EPR intensity, can be identified in the EPR spectrum (Figure 1b). This spectrum can be attributed to a single paramagnetic species and will hereafter be labeled species A. We will only consider the nature and identity of species A in this work. This signal bears all the characteristics of a cobalt-bound radical species. Note that the radical species is extremely robust; it is still present after 5 years of storage in air. The W-band CW-EPR spectrum of species A (Figure 2c) facilitates the clear determination of the principal *g* values, where the cobalt hyperfine interaction is only resolved in the X-band CW-EPR spectrum (Figure 2a, eight-line pattern due to interaction with ^{59}Co [I = 7/2]). The EPR parameters obtained by simulation of these spectra are shown in Table 1. The principal *g* values are typical for an organic radical, while the cobalt hyperfine coupling indicates that only a small part of the electron spin density from the radical is delocalized toward the cobalt center.

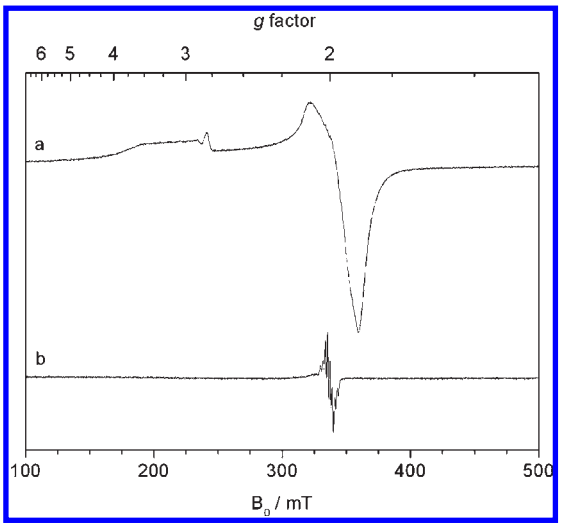

Figure 1. X-band CW-EPR spectra of a frozen toluene solution of (a) (*R*,*R*)-[Co(**1**)] and (b) (*R*,*R*)-[Co(**1**)] after addition of acetic acid (10 equiv) under aerobic conditions (30 min). The spectra were recorded at 100 K.

Experimental Evidence for a Coordinated Phenoxyl Radical. From the experimental EPR data, it appears that an organic-type radical is responsible for the signal in Figures 1b and 2. In principle, this radical could be localized on the ligand **1** itself (for example, as a coordinated phenoxyl radical) or alternatively on a possible ligating paramagnetic acetate moiety (since the complex is activated using acetic acid). Several points, however, argue against the latter assumption. First, upon the addition of formic acid to (*R*,*R*)-[Co(**1**)] under air, the same X-band CW-EPR spectrum, albeit with lower intensity, is obtained compared to activation using acetic acid (see the Supporting Information). Second, the X-band CW-EPR spectrum of species A (Figure 2a) resembles that of previously reported phenoxyl-radical-ligated Co^{III}-salen complexes[35−37] (Table 1). Third, the formation of a phenoxyl radical, as opposed to a bound (ligating) substrate-based radical, is confirmed by resonance Raman (RR) experiments.

It was shown previously that RR spectroscopy can be used to identify phenoxyl radical species.[38] By excitation of the $\pi \rightarrow \pi^*$ transition of the radical (412 nm), the Raman intensities of the phenoxyl vibrations are selectively enhanced. In particular, the ν_{7a} (predominantly

(26) Schafer, A.; Horn, H.; Ahlrichs, R. *J. Chem. Phys.* **1992**, *97*, 2571–2577.
(27) Dill, J. D.; Pople, J. A. *J. Chem. Phys.* **1975**, *62*, 2921–2923.
(28) Hehre, W. J.; Ditchfie., R; Pople, J. A. *J. Chem. Phys.* **1972**, *56*, 2257.
(29) Krishnan, R.; Binkley, J. S.; Seeger, R.; Pople, J. A. *J. Chem. Phys.* **1980**, *72*, 650–654.
(30) Barone, V. In *Recent Advances in Density Functional Methods*; Chong, D. P., Ed.; World Scientific Publ. Co.: Singapore, 1996; p 287.
(31) Sinnecker, S.; Rajendran, A.; Klamt, A.; Diedenhofen, M.; Neese, F. *J. Phys. Chem. A* **2006**, *110*, 2235–2245.
(32) Reynolds, J. A.; Hough, J. M. *Proc. Phys. Soc. London, Sect. B* **1957**, *70*, 769–775.
(33) Vinck, E.; Van Doorslaer, S.; Murphy, D. M.; Fallis, I. A. *Chem. Phys. Lett.* **2008**, *464*, 31–37.
(34) Daul, C.; Schläpfer, C. W.; von Zelewsky, A. *Struct. Bond.* **1979**, *36*, 129–171.
(35) Canevali, C.; Orlandi, M.; Pardi, L.; Rindone, B.; Scotti, R.; Sipila, J.; Morazzoni, F. *J. Chem. Soc., Dalton Trans.* **2002**, 3007–3014.
(36) Zombeck, A.; Drago, R. S.; Corden, B. B.; Gaul, J. H. *J. Am. Chem. Soc.* **1981**, *103*, 7580–7585.
(37) Bolzacchini, E.; Canevali, C.; Morazzoni, F.; Orlandi, M.; Rindone, B.; Scotti, R. *J. Chem. Soc., Dalton Trans.* **1997**, 4695–4699.
(38) Muller, J.; Kikuchi, A.; Bill, E.; Weyhermuller, T.; Hildebrandt, P.; Ould-Moussa, L.; Wieghardt, K. *Inorg. Chim. Acta* **2000**, *297*, 265–277.

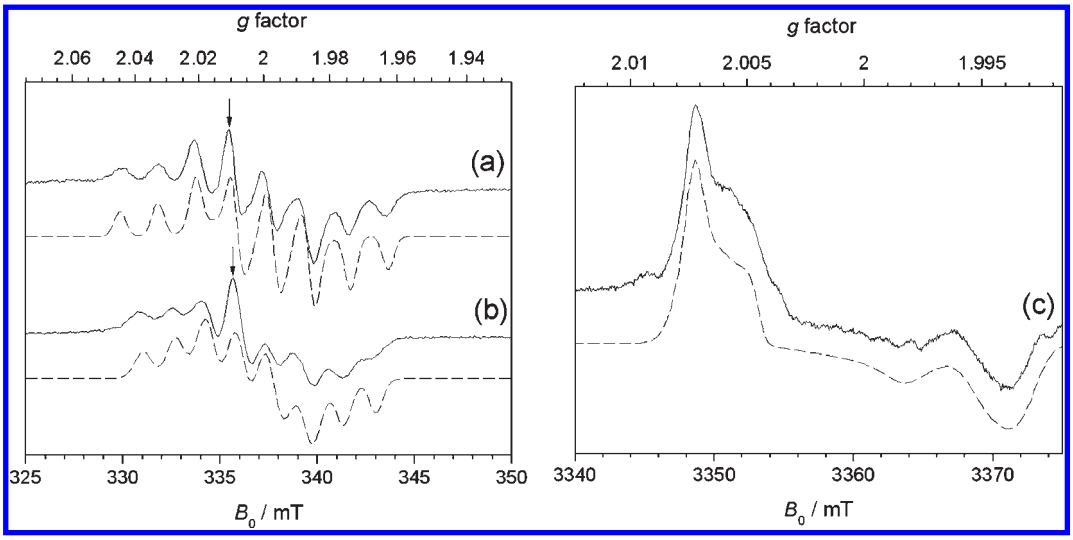

Figure 2. Experimental (full line) and simulated (dashed line) X-band (a,b) and W-band (c) CW-EPR spectra of a frozen toluene solution of (a, c) (*R*,*R*)-[Co(**1**)] after addition of acetic acid (10 equiv) under air (species A) and (b) after addition of 60 equiv of pyridine to a (species B). The spectra were recorded at a temperature of 100 K. The arrows indicate the observer positions at which the HYSCORE spectra in Figure 4 were recorded.

Table 1. Principal *g* and ^{59}Co Hyperfine Values Obtained from Simulations of the CW-EPR Spectra of Species A, Species B, Pyridine-Ligated Oxygenated (*R*,*R*)-[Co(**1**)], Mono-Pyridine-Ligated (*R*,*R*)-[Co(**1**)], and Bis-pyridine-Ligated (*R*,*R*)-[Co(**1**)], Compared to Those Found for Related Systems[a]

	g_x	g_y	g_z	$\lvert A_{x'}^{Co}\rvert$ (MHz)	$\lvert A_{y'}^{Co}\rvert$ (MHz)	$\lvert A_{z'}^{Co}\rvert$ (MHz)	ref
species A[b]: [Co^{III}(**1**$^{\bullet}$)-(OAc)$_{1,2}$](OAc)$_{1,0}$	2.0060 (±0.0005)	2.0031 (±0.0004)	1.9943 (±0.0002)	17 (±2)	55 (±5) (α, β, γ) = (0° ± 10°, 0°,[c] 0° ± 10°)	14 (±2)	this work
[Co^{III}(salen)(RO^{-})(RO$^{\bullet}$)][d]	2.002	2.002	2.002	14	52	14	35
species B: [Co^{III}(**1**$^{\bullet}$)(Py)$_2$]$^{2+e}$	2.006 (±0.010)	2.001 (±0.001)	1.994 (±0.010)	15 (±10)	47 (±2)	10 (±5)	this work
[Co(**1**)(Py)][f]	2.46 (±0.01)	2.20 (±0.01)	2.01 (±0.01)	±135 (±5)	±40 (±5) $\lvert A^{N}\rvert$ = 40 ± 5 MHz	±279 (±5)	this work
[Co(**1**) (Py)$_2$][f]	2.33 (±0.01)	2.215 (±0.01)	1.98 (±0.01)	±30 (±5)	±60 (±5) $\lvert A^{N}\rvert$ = 40 ± 5 MHz	±230 (±5)	this work
[(Py)Co^{III}(**1**)O$_2^{-}$][e]	2.006 (±0.010)	1.990 (±0.005)	2.075 (±0.005)	55 (±5)	20 (±5) (α, β, γ) = (0°, 60° ± 10°, 0°)	38 (±5)	this work

[a] All [Co(**1**)] complexes listed in the table are of the (*R*,*R*) enantiomer. [b] Toluene solution. [c] Value could not be determined accurately. [d] Chloroform solution, RO^{-} is the anion of methyl-E ferulate (a phenol compound), RO$^{\bullet}$ is the corresponding phenoxyl radical. [e] In a 2:1 mixture of toluene and pyridine. [f] In a 10:1:5 mixture of toluene, acetic acid, and pyridine.

ν(C−O)) and the ν_{8a} (predominantly ν(C═C)) modes at ∼1500 cm^{-1} and ∼1600 cm^{-1}, respectively, are sensitive markers for phenoxyl radical species. In Figure 3, the RR spectra of both the precatalyst (*R*,*R*)-[Co(**1**)] complex and the subsequent acid-activated complex are shown. The peak at ∼1530 cm^{-1} may be assigned to the ν_{7a} mode. The ν_{8a} mode is visible at 1636 cm^{-1} and is strongly enhanced in the activated complex. The value of 1636 cm^{-1} for ν_{8a} is rather high, and together with the fact that the ν_{7a} mode is less intense than the ν_{8a} mode, these RR observations are nevertheless characteristic of metal-coordinated phenoxyl radicals.[38]

All of the previous observations indicate that species A stems from a cobalt-bound phenoxyl radical. However, at this stage, the precise formal representation of the radical must be carefully considered, i.e., classified either as a [Co^{III}(**1**$^{\bullet}$)(OAc)$_n$]$^{m+}$-type radical (n = 0, 1, or 2; m = 2, 1, or 0) or a [Co^{III}(**1**)(**1**$^{\bullet}$H)(OAc)$_{n=0,1}$]$^{m+}$-type radical (m = 2, 1), the latter nomenclature suggesting that the axially bound phenoxyl radical species originates from the free H$_2$(**1**) ligand or a salicylaldehyde ligand hydrolysis product. In this context, it is important to note that all phenoxyl-radical-ligated Co^{III}−salen complexes observed to date were obtained by the addition of phenols or quinones to the Co^{II} salen complexes.[35−37] In order to further elucidate the nature of species A, several additional experiments were therefore performed.

First, the X-band CW-EPR spectra of a toluene solution of species A were recorded at variable temperatures and analyzed (see the Supporting Information). The temperature-dependent spectra can be simulated by only varying a single correlation time. This implies that the motion of the radical is governed by the temperature-dependent motion of the entire complex itself, indicating that the radical is indeed purely ligand based. In the hypothetical case where the radical is an axially bound species, a more complex motional behavior would be expected (i.e., a combination of a rotation around the Co−X$^{\bullet}$ axis, where X$^{\bullet}$ is the axially

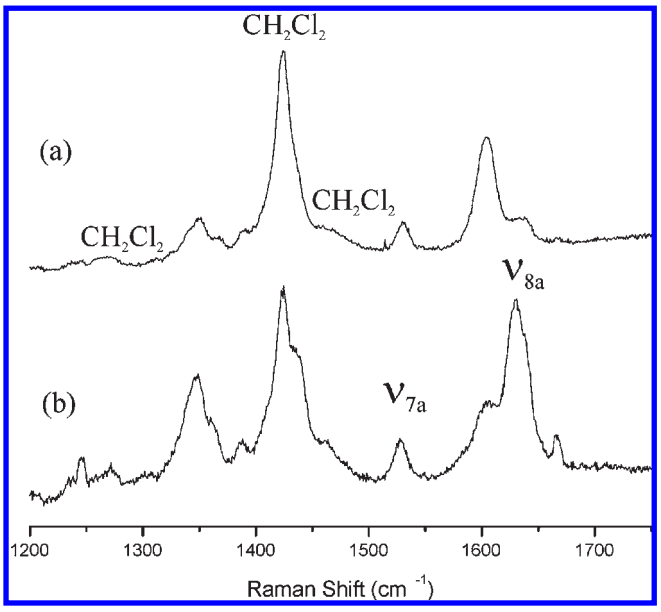

Figure 3. Resonance Raman spectra of (a) (*R*,*R*)-[Co(**1**)], dissolved in a mixture of 50% toluene and 50% dichloromethane, and (b) activated [Co(**1**)], dissolved in a mixture of 50% toluene and 50% dichloromethane. The Raman peaks due to the dichloromethane solvent, the ν_{7a} and ν_{8a} stretching modes, are indicated. The spectra were recorded with a laser power of 10 mW, and with an excitation wavelength of 413 nm.

bound species, plus the overall molecular motion of the entire adduct[39,40]).

To further substantiate this proposition, a series of experiments were performed in order to displace any possible axially bound radical species by substitution with a stronger axial donor. The donor chosen was pyridine (Py). Pyridine (60 equiv) was therefore added to a toluene solution of the precatalyst (*R*,*R*)-[Co(**1**)] complex with 10 equiv of acetic acid, first under a N_2 atmosphere and second under air. In our previous work, we have shown that the addition of 10 equiv of acetic acid under N_2 results in the formation of acetate-/acetic acid-ligated [Co(**1**)] complexes.[33] Subsequent addition of pyridine under N_2 proves unambiguously that pyridine can substitute and replace acetate/acetic acid as an axial donor ligand in the parent (*R*,*R*)-[Co(**1**)] complex (see the Supporting Information). Both mono and bis-pyridine-ligated (*R*,*R*)-[Co^{II}(**1**)$(Py)_{n=1,2}$] adducts (and a minor contribution of oxygenated pyridine-ligated (*R*,*R*)-[Co(**1**)(Py)O_2]) are thus formed. The corresponding EPR parameters for these adducts are given in Table 1. By comparison, the addition of pyridine to the activated (*R*,*R*)-[Co(**1**)] complex (i.e., activated under aerobic conditions) induced a smaller change in the X-band CW-EPR spectrum of species A (as shown in Figure 2b). Although the observed change indicates that pyridine ligation has occurred with the phenoxyl radical (producing a pyridine-bound phenoxyl radical, labeled species B in Table 1 and Scheme 1), the strong resemblance of the CW-EPR spectra of A and B shows that no major structural rearrangement has taken place. Figure 4 compares the nitrogen HYSCORE spectra of species A and B, taken at the observer position indicated with an arrow in Figure 2a and b, respectively. While the nitrogen HYSCORE spectrum of species A is dominated by the HYSCORE peaks of the diamine backbone ^{14}N nuclei of ligand **1** in the (+,+) quadrant, indicative of a weak nitrogen coupling, the spectrum of species B is clearly different, showing features in both quadrants. These peaks arise from the interactions with the ^{14}N nucleus of pyridine. Note that the peaks of the ligand ^{14}N nuclei are partially overlapping with these new peaks (see the Supporting Information). Furthermore, the ligand **1** ^{14}N HYSCORE peaks are largely suppressed by the modulations of the strongly coupled pyridine nuclei, as is confirmed by simulations (see the Supporting Information). These types of suppression effects are common in ESEEM experiments.[41]

The hyperfine interaction of the pyridine ^{14}N nuclei is approximately twice the nitrogen Larmor frequency (exact cancellation). In this cancellation case, the ESEEM frequencies in one M_S manifold are close to the true nuclear-quadrupole frequencies[42]

$$\nu_+ = K(3+\eta),\ \nu_- = K(3-\eta) \text{ and } \nu_0 = 2K\eta \quad (2)$$

with the quadrupole-coupling constant $K = e^2qQ/(4h) = P_3/2$, and the asymmetry parameter $\eta = (P_1 - P_2)/P_3$, where P_1, P_2, and P_3 are the nuclear-quadrupole principal values ($|P_1| < |P_2| < |P_3|$). These three nuclear quadrupole frequencies correlate with the double-quantum (dq) frequency of the other M_S manifold in the HYSCORE spectrum (Figure 4b). The observation of cross peaks at ($-2\nu_+$, dq_α) and ($2\nu_-$, dq_α) indicates that two equivalent nitrogen nuclei are observed; i.e., two pyridine molecules ligate axially to the cobalt ion (Scheme 1, species B). This experimental observation proves unambiguously that species A must be ligand **1**-based (i.e., [Co^{III}(**1**$^\bullet$)]$^{2+}$-based), and the source of the paramagnetism cannot arise from any axially bound substrate radical. The hyperfine and nuclear-quadrupole tensor of the coordinated pyridine nitrogens of species B and the corresponding HYSCORE simulations are shown in the Supporting Information. Note that these nuclear-quadrupole values are in good agreement with those of other metal-coordinated pyridine complexes[43,44] (Supporting Information). The values are significantly smaller than those of free pyridine.[43] It was already reported earlier that coordination of a Lewis acid to the lone pair of the pyridine nitrogen decreases the electric field gradient significantly.[43]

DFT Computations of the Coordinated Phenoxyl Radical. Since we previously established that acetate/acetic acid binds to (*R*,*R*)-[Co(**1**)] under a N_2 atmosphere,[33] and since the acid plays a crucial role in the activation of the catalyst, it is highly likely that some acetate/acetic acid also binds to the cobalt(III)−phenoxyl radical ([Co^{III}(**1**$^\bullet$)]$^{2+}$). To clarify this issue, DFT computations were performed.

(39) Bowen, J. H.; Shokhirev, N. V.; Raitsimring, A. M.; Buttlaire, D. H.; Walker, F. A. *J. Phys. Chem. B* **1997**, *101*, 8683–8691.
(40) Walker, F. A.; Bowen, J. *J. Am. Chem. Soc.* **1985**, *107*, 7632–7635.
(41) Stoll, S.; Calle, C.; Mitrikas, G.; Schweiger, A. *J. Magn. Reson.* **2005**, *177*, 93–101.
(42) Flanagan, H. L.; Singel, D. J. *J. Chem. Phys.* **1987**, *87*, 5606–5616.
(43) Hsieh, Y. N.; Rubenacker, G. V.; Cheng, C. P.; Brown, T. L. *J. Am. Chem. Soc.* **1977**, *99*, 1384–1389.
(44) Jorin, E.; Rudin, M.; Schweiger, A.; Gunthard, H. H. *Chem. Phys. Lett.* **1980**, *69*, 193–197.

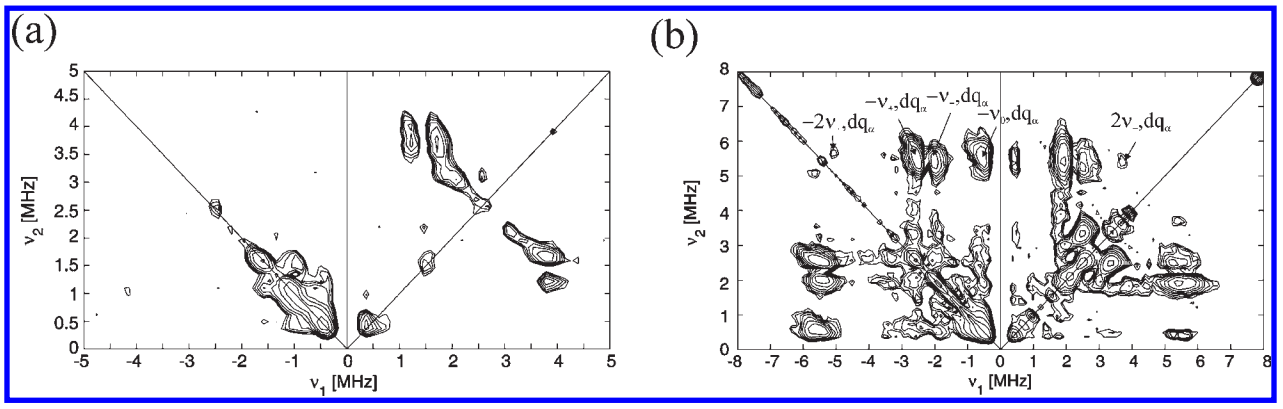

Figure 4. X-band HYSCORE spectra recorded at a magnetic-field position corresponding with $g \sim 2.0031$ (position indicated with an arrow in Figure 2a, b) of a frozen toluene solution of (a) species A and (b) species B. The spectra were recorded at 30 K and with a τ value of 176 ns (a) and 104 ns (b).

Our experimental (spectroscopic) evidence clearly shows that species A must be a Co^{III}-bound phenoxyl radical, since a Co^{II}-bound radical would lead to a completely different CW-EPR spectrum. In other words, a two-electron oxidation process must have occurred during activation in order to generate the Co^{III}-bound phenoxyl radical. Therefore, DFT computations were initially performed on three different models of oxidized (*R*,*R*)-[Co(**1**)] complexes, namely, (*a*) $[Co(\mathbf{1})]^{2+}$, (*b*) acetate-ligated $[Co(\mathbf{1})(OAc)]^{+}$, and (*c*) bis-acetate-ligated $[Co(\mathbf{1})(OAc)_2]$. In essence, these cases represent coordination sphere isomers of the system in question. Figure 5 shows the computed spin densities for these three complexes, and the full analysis is given in the Supporting Information. For $[Co(\mathbf{1})]^{2+}$, the spin density is evenly delocalized over the ligand **1** (Figure 5a). The computed principal *g* and cobalt hyperfine values (Table 2) are typical for an unpaired electron that is mainly localized on the cobalt ion (d_{z^2} ground state); this clearly contradicts the experimental findings for species A where the spin is not localized on cobalt. This is not unexpected since a four coordinate Co^{III} species would be extremely Lewis acidic and would tend to increase its coordination number by interaction with available acetate ligands. For the monoacetate adduct (*b*) $[Co(\mathbf{1})(OAc)]^{+}$, the spin density is now unevenly distributed toward one of the phenoxyl groups of the ligand **1**, and this important result agrees with the experimental data (Figure 5b). The experimental principal *g* values listed in Table 1 are better reproduced, and the computed spin density distribution is in good agreement with previous experiments on various free phenoxyl radicals.[45,46] In solution, the formula of this species would thus be described as $[Co^{III}(\mathbf{1}^{\bullet})(OAc)](OAc)$.

Although the calculated cobalt hyperfine values of model *b*, $[Co(\mathbf{1})(OAc)]^{+}$ (Table 2), already reflect the experimental trends, the experimental and theoretical results are in fact best reconciled on the basis of the bis-acetate $[Co(\mathbf{1})(OAc)_2]$ model (*c*). Here, the spin density is mainly localized on one of the two phenoxyl groups (Figure 5c), and hence the formula of the solution species may be written as the valence-localized phenoxyl $[Co^{III}(\mathbf{1}^{\bullet})(OAc)_2]$. The magnitude of the computed *g* and cobalt hyperfine values are comparable to the experiment, although there are still important differences for the cobalt hyperfine values (Table 2). Nevertheless, the DFT computations confirm that a cobalt-bound phenoxyl radical is indeed stable and indicate that acetate ligation (whether mono- or bis-acetate) plays an important function in the spin distribution.

Is There Direct Evidence of Acetate Ligation to the Phenoxyl Radical ? The CW-EPR and HYSCORE spectra of (*R*,*R*)-[Co(**1**)], activated with ^{13}C-labeled acetic acid, were measured in order to confirm the presence/absence, and possibly number, of axially bound acetate molecules in species A. However, no traces of a ^{13}C contribution were found in these spectra (see the Supporting Information). Although this may indicate a lack of acetate ligation, it is likely that the hyperfine interaction is too small to be detected and/or that this coupling is suppressed by cross-suppression effects known to occur in ESEEM experiments.[41] The HYSCORE experiment performed on species B, i.e., the pyridine-ligated phenoxyl radical (Figures 2b and 4b), revealed that only a small amount of spin density is centered on the pyridine nitrogen ($|a_{iso}| = 2.7$ MHz), indicating a maximum of 0.17% spin density on the ^{14}N nucleus ($\rho_N = a_{iso}/a_0$ with $a_0 = 1538.22$ MHz).[47] Hence, the ^{13}C coupling in an acetate-ligated phenoxyl radical (species A) would be expected to be essentially dipolar. The DFT model predicts an $O^{\bullet}_{Phenoxyl}-{}^{13}C$ distance of $\sim$0.32 nm, which in a pure point-dipolar approximation corresponds to [−0.6, −0.6, 1.2] MHz. However, the electron spin density is not centered exclusively on the oxygen atom ($O_{Phenoxyl}$), but delocalized over the phenoxyl ring, and thus, the predicted coupling is likely to be even smaller. In fact, the DFT computations of model (*c*), $[Co(\mathbf{1})(OAc)_2]$, predict an anisotropic part of [−0.65, 0, 0.65] MHz. As shown in the Supporting Information, ^{13}C ESEEM contributions with small anisotropic parts may be suppressed by the strong ^{14}N modulations.

Comparing the Experimental and Computed Spin Hamiltonian Values. From the comparison of Tables 1 and 2, it is obvious that, although the computed principal *g* and cobalt hyperfine values of model (*c*) corroborate the phenoxyl radical model, there is not an exact match between the theoretical and the experimental values. It has been shown before that the current state-of-the-art DFT

(45) Tommos, C.; Tang, X. S.; Warncke, K.; Hoganson, C. W.; Styring, S.; McCracken, J.; Diner, B. A.; Babcock, G. T. *J. Am. Chem. Soc.* **1995**, *117*, 10325–10335.
(46) Warncke, K.; Babcock, G. T.; McCracken, J. *J. Am. Chem. Soc.* **1994**, *116*, 7332–7340.
(47) Koh, A. K.; Miller, D. J. *At. Data Nucl. Data Tables* **1985**, *33*, 235–253.

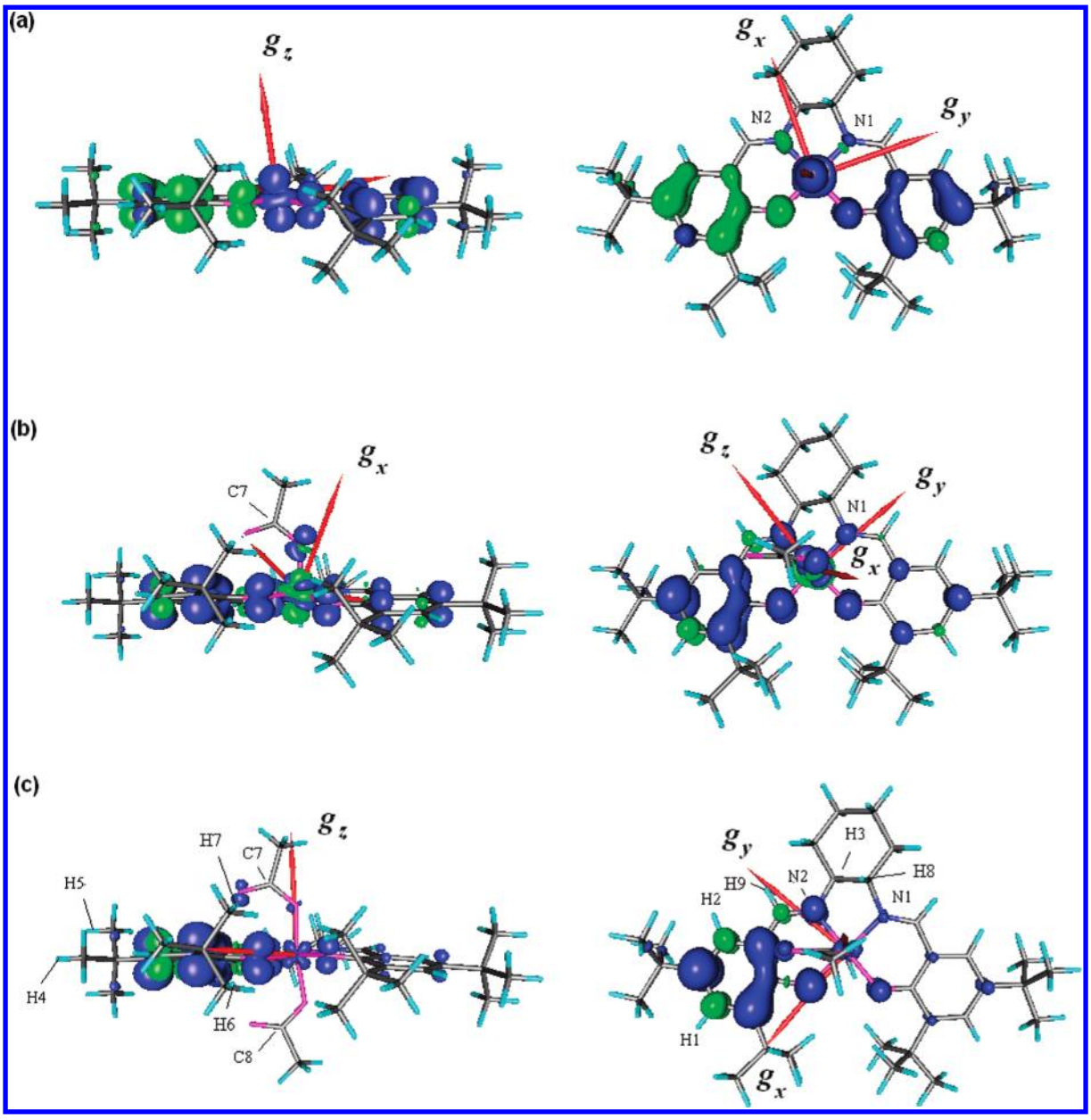

Figure 5. Computed spin density of (*a*) $[Co(\mathbf{1})]^{2+}$, (*b*) $[Co(\mathbf{1})(OAc)]^{+}$, and (*c*) $[Co(\mathbf{1})(OAc)_2]$. Blue represents positive spin density, while green represents negative spin density. The arrows indicate the computed principal *g* axes. The protons H1−H9, carbons C7 and C8, and nitrogens N1 and N2 are indicated.

Table 2. DFT-Computed Principal *g* and ^{59}Co Hyperfine Values for (*a*) $[Co(\mathbf{1})]^{2+}$, (*b*) $[Co(\mathbf{1})(OAc)]^{+}$, and (*c*) $[Co(\mathbf{1})(OAc)_2]$[a]

		g_x	g_y	g_z	A_1^{Co} (MHz)	A_2^{Co} (MHz)	A_2^{Co} (MHz)
(*a*)	$[Co(\mathbf{1})]^{2+}$	2.4177	2.3448	2.0109	438	364	652
(*b*)	$[Co(\mathbf{1})(OAc)]^{+}$	2.0125	1.9604	1.9394	−158	−49	−4
(*c*)	$[Co(\mathbf{1})(OAc)_2]$	2.0098	2.0083	1.9949	−40	−10	−4

[a] The cobalt hyperfine values were computed with the basis set CPIII(Co)/EPRIII(N)/TZVP(C,H). The *g* values were computed with the basis set TZVP (Co)/6_31 (other atoms).

methods still struggle to exactly reproduce the *g* and metal hyperfine values of this type of system.[48−50] Since we are dealing here with a system whereby the spin density is distributed strongly over the ligand **1** and the cobalt center, considerable differences between the experimental and theoretical interactions of the unpaired electron with the ^{14}N and ^{1}H nuclei of ligand **1** can also be expected.

The DFT computations of model (*c*), $[Co(\mathbf{1})(OAc)_2]$, predict a weak coupling with one of the two ligand nitrogen nuclei, labeled N1, and a larger interaction with the other ^{14}N nucleus, labeled N2 (Table 3). Table 3 also lists the computed hyperfine values for protons H1−5.

(48) Neese, F. *J. Biol. Inorg. Chem.* **2006**, *11*, 702–711.
(49) Neese, F.; Munzarova, M. L. In *Calculation of NMR and EPR Parameters*; Kaupp, M., Buhl, M., Malkin, V. G., Eds.; Wiley-VCH: Weinheim, Germany, 2004; p 21.
(50) Stein, M.; van Lenthe, E.; Baerends, E. J.; Lubitz, W. *J. Am. Chem. Soc.* **2001**, *123*, 5839–5840.

Table 3. ^{14}N Hyperfine and Nuclear Quadrupole Values and ^{1}H Hyperfine Values Obtained by DFT Computations for [Co(**1**)(OAc)$_2$][a]

	A_1 (MHz)	A_2 (MHz)	A_3 (MHz)	P_1 (MHz)	P_2 (MHz)	P_3 (MHz)
N1	−0.53	−0.75	1.33	−0.17	−0.73	0.90
N2	−0.03	0.4	10.26	0.27	0.75	−1.02
H1	5.90	10.15	4.05			
H2	7.25	4.31	2.09			
H3	13.83	11.52	11.34			
H4	5.99	8.67	6.44			
H5	5.90	8.57	6.35			

[a] Only the values for protons H1−H5 are given (the values for the other protons are given in the Supporting Information). The numbering of the nuclei is given in Figure 5. The nitrogen hyperfine and nuclear-quadrupole values were computed with the basis set CPIII(Co)/EPRIII-(N)/TZVP(C,H). The proton hyperfine values were computed with the basis set CP(Co)/EPRII(N,H)/6_31(C). p = 1, 3.

The hyperfine interaction theoretically predicted for proton H3 is clearly overestimated, since proton hyperfine couplings with $a_{iso} \geq 11$ MHz would be observable in the room-temperature CW-EPR spectrum of species A (see Supporting Information). In agreement with this, X-band ^{1}H HYSCORE reveals a maximum ^{1}H coupling of ∼8 MHz for species A (Figure 6a). The X-band ^{1}H Mims ENDOR spectra (Figure 6b and Supporting Information) corroborate the conclusion that the ^{1}H hyperfine values are overestimated in the DFT model (*c*). The signals seen in the [5−10] MHz region in the Mims ENDOR stem from the ^{59}Co contribution (see further analysis, Davies ENDOR).

As mentioned earlier, the HYSCORE experiments reveal a weak ^{14}N interaction (Figure 4a). These HYSCORE spectra can be simulated assuming the contributions of one or two ^{14}N nuclei with $|a_{iso}| = 1.1 \pm 0.3$ MHz, $|e^2qQ/h| = 1.65 \pm 0.3$ MHz, and $\eta = 0.6 \pm 0.2$ (see the Supporting Information). While the experimental spin Hamiltonian data lie in the order of what is predicted theoretically for N1, the computed isotropic and dipolar hyperfine couplings of nitrogen N2 are much larger than the experimental values. Several experiments were set up to detect such a large ^{14}N coupling. In a first instance, simulations of the CW-EPR spectra revealed that the computed EPR parameters of N2 are too small to be directly verified by CW EPR (see the Supporting Information). Figure 6c shows the X-band Davies ENDOR spectrum obtained using strong mw pulses in order to suppress the contributions of the weakly coupled nuclei. The spectrum can be well reproduced assuming only the ^{59}Co hyperfine interaction and a ^{59}Co nuclear quadrupole coupling of $|e^2qQ/h| = 90 \pm 10$ MHz and $\eta = 0.7 \pm 0.4$ (Figure 6c). ^{59}Co nuclear quadrupole values on the same order have been observed for Co(II)(acacen) ($e^2qQ/h = -116$ MHz).[51] There was no need to assume an interaction with a strongly coupled ^{14}N nucleus to explain the Davies ENDOR spectrum. Furthermore, X-band matched HYSCORE and W-band ELDOR-detected NMR experiments also proved unsuccessful at detecting a contribution of a strongly coupled ^{14}N nucleus. This points to the possibility that also the contribution N2 is not correctly represented by the DFT computations.

The computed proton hyperfine values of [Co(**1**)(OAc)$_2$] can also be compared with those for free (noncoordinated) phenoxyl radicals, which have been extensively studied.[35] The hyperfine couplings of protons H1 and H2 in the aromatic ring of [Co(**1**)(OAc)$_2$] compare favorably with the experimental hyperfine values of [4.76, 7.57, 1.12] MHz found for C2′−H and C6′−H in a tyrosine radical.[45,46,52]

Discussion

Phenoxyl Co^{III} species based on phenolate macrocyclic complexes have been widely reported and investigated by numerous techniques including EPR, CV, UV−vis, and resonance Raman.[3−5] Wieghardt et al.[53] reported well resolved room temperature spectra of the phenoxyl−cobalt(III) species with $g_{iso} = 2.0047$ and hyperfine coupling to the ^{59}Co nucleus of $a_{Co} = 9.8$ MHz. Of more relevance to the current work are the coordinated phenoxyl radicals based on the tetradentate Schiff bases which contain phenolate pendant arms in the ligand structure. Shimazaki et al.[54] studied the electrochemical oxidation of [Ni(**1**)]. At a low temperature (123 K), a Ni^{III}−phenolate complex was easily identified by EPR, on the basis of the characteristic rhombic *g* tensor typical of a low spin ^{2}A$_1$ (d_{z^2}) ground state. However, at elevated temperatures, between 158 and 173 K, this rhombic signal evolved into an isotropic EPR signal with $g_{iso} = 2.04$, which was assigned to the Ni^{II}−phenoxyl radical, indicating the tautomerism that can exist between the two redox states ([Ni^{III}(**1**)]$^+$ or [Ni^{II}(**1**$^{\bullet}$)]$^+$). Most recently, Rotthaus et al.[55,56] extended this study to a range of closely related Schiff base Ni^{II} complexes, proving the formation of the Ni^{II}−phenoxyl radical with partial delocalization of the SOMO onto the metal orbitals, and this has since been confirmed in several further studies.[7,57,58] Pratt and Stack have also generated and characterized the coordinated phenoxyl radical in [Cu^{II}(**1**)] (labeled [Cu^{II}(**1**$^{\bullet}$)]$^+$) as a biomimetic model for galactose oxidase complexes.[6] The EPR data reported in their study was consistent with the formation of an antiferromagnetically coupled Cu^{II}−phenoxyl complex, analogous to that found in the oxidized form of GOase. Oxidation of the Cu^{II} complex to Cu^{II}−phenoxyl simply resulted in an attenuation of the original Cu^{II} EPR signal by ∼15%.[6]

It is therefore clear that coordinated phenoxyl radicals based on metal complexes of ligand **1** are well-known, at least for Cu and Ni. To date, no evidence has been presented in the literature for the existence of a cobalt-based phenoxyl radical of **1** (Table 1). Although Canevali et al.[35] have reported the formation of a cobalt−phenoxyl radical based on the structurally related [Co(salen)] ligand, their radical originated entirely from a ligated substrate, namely, [Co^{III}(salen)(RO$^-$)-(RO$^{\bullet}$)]$^+$. The experimental work presented here has therefore

(51) Rudin, M.; Schweiger, A.; Berchten, N.; Gunthard, H. H. *Mol. Phys.* **1980**, *41*, 1317–1328.

(52) Hulsebosch, R. J.; van den Brink, J. S.; Nieuwenhuis, S. A. M.; Gast, P.; Raap, J.; Lugtenburg, J.; Hoff, A. J. *J. Am. Chem. Soc.* **1997**, *119*, 8685–8694.

(53) Sokolowski, A.; Adam, B.; Weyhermuller, T.; Kikuchi, A.; Hildenbrand, K.; Schnepf, R.; Hildebrandt, P.; Bill, E.; Wieghardt, K. *Inorg. Chem.* **1997**, *36*, 3702–3710.

(54) Shimazaki, Y.; Tani, F.; Fukui, K.; Naruta, Y.; Yamauchi, O. *J. Am. Chem. Soc.* **2003**, *125*, 10512–10513.

(55) Rotthaus, O.; Jarjayes, O.; Del Valle, C. P.; Philouze, C.; Thomas, F. *Chem. Commun.* **2007**, 4462–4464.

(56) Rotthaus, O.; Labet, V.; Philouze, C.; Jarjayes, O.; Thomas, F. *Eur. J. Inorg. Chem.* **2008**, 4215–4224.

(57) Benisvy, L.; Kannappan, R.; Song, Y. F.; Milikisyants, S.; Huber, M.; Mutikainen, I.; Turpeinen, U.; Gamez, P.; Bernasconi, L.; Baerends, E. J.; Hartl, F.; Reedijk, J. *Eur. J. Inorg. Chem.* **2007**, 637–642.

(58) Shimazaki, Y.; Yajima, T.; Tani, F.; Karasawa, S.; Fukui, K.; Naruta, Y.; Yamauchi, O. *J. Am. Chem. Soc.* **2007**, *129*, 2559–2568.

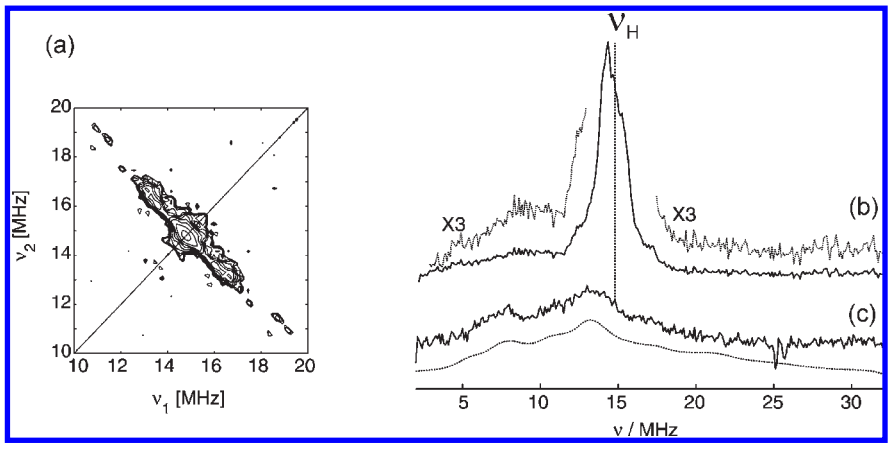

Figure 6. Different HYSCORE and ENDOR spectra of a frozen toluene solution of (*R*,*R*)-[Co(**1**)] after the addition of acetic acid (10 equiv) under air (standard activation conditions). All spectra were recorded at a magnetic-field position corresponding to $g = g_y$. (a) Experimental X-band matched HYSCORE spectrum ($T = 30$ K) with matched pulse lengths of 48 ns and interpulse distance $\tau = 128$ ns. The spectrum is symmetrized. (b) X-band Mims ENDOR spectrum representing a sum of Mims ENDOR spectra recorded with τ values of 96 ns, 112 ns, 136 ns, 176 ns, and 192 ns. The individual Mims ENDOR spectra are shown in the Supporting Information. (c) Experimental (top) and simulated (bottom) X-band Davies ENDOR spectrum recorded using strong mw pulse ($t_\pi = 48$ ns) and short rf length (5.4 μs). All ENDOR spectra were recorded at 4 K.

provided for the first time a sound basis for proving the existence of the coordinated cobalt(III)−phenoxyl radical $[Co^{III}(\mathbf{1}^{\bullet})(OAc)_n](OAc)_m$ ($n = m = 1$ or $n = 2$, $m = 0$). The well resolved EPR spectra facilitated the clear identification of the spin Hamiltonian parameters ($g_x = 2.0060$, $g_y = 2.0031$, $g_z = 1.9943$, $A_x = 17$ MHz, $A_y = 55$ MHz, $A_z = 14$ MHz). What is remarkable is that this species is generated during the activation of a widely used HKR catalyst (albeit in low levels of 1−2%), unlike the situation for $[Ni^{II}(\mathbf{1}^{\bullet})]^+$ and $[Cu^{II}(\mathbf{1}^{\bullet})]^+$ where the radicals were generated electrochemically.

It should be recalled that the experimental evidence for $[Co^{III}(\mathbf{1}^{\bullet})]^{2+}$ was based on the EPR, HYSCORE, RR, and DFT results. The spin Hamiltonian parameters presented in Table 1 are consistent with this assignment, with the notable small hyperfine coupling to ^{59}Co and small *g* anisotropy expected of an essentially organic radical. The RR results, particularly the ν_{8a} and ν_{7a} sensitive markers at 1636 and 1530 cm^{-1}, proved conclusively the presence of a coordinated phenoxyl radical, as opposed to a bound (ligating) substrate based radical. The latter proposal was also proved using pyridine as a stronger substrate to displace any axially ligating species such as AcO^- or a bound radical. The HYSCORE data revealed cross peaks at ($-2\nu_+$, dq_α) and ($2\nu_-$, dq_α), indicative of two equivalent ^{14}N nuclei, which can only be explained as arising from the presence of the $[Co^{III}(\mathbf{1}^{\bullet})(Py)_2]^{2+}$ adduct, labeled species B. This experiment proved that the radical was ligand based rather than substrate based. To ascertain whether acetate/acetic acid was indeed bound to species A, HYSCORE experiments were performed using ^{13}C labeled HOAc but revealed no signals arising from ^{13}C couplings. On the basis of the theoretically predicted small ^{13}C coupling and the observed small magnitude of the ^{14}N coupling from the coordinated Py in $[Co^{III}(\mathbf{1}^{\bullet})(Py)_2]^{2+}$, the absence of these ^{13}C signals was not unexpected (see the Supporting Information).

Although the experiments could not categorically confirm the presence or absence of coordinated acetate in Co phenoxyl complexes of **1**, its presence is likely under the acetic acid conditions employed, suggesting that species A should be formally labeled as $[Co^{III}(\mathbf{1}^{\bullet})(OAc)_{1,2}](OAc)_{1,0}$. DFT calculations were therefore used to probe the nature of the Co phenoxyl radical and, as evidenced in the Results section (Table 2 and Figure 5), not only indicate the stability of $[Co^{III}(\mathbf{1}^{\bullet})(OAc)_2]$ but also predict the correct order of magnitude of the cobalt hyperfine values and small *g* anisotropy. However, the agreement is only qualitative. This is also the case for the hyperfine values of the ligand nuclei (Table 3). The proton hyperfine couplings were clearly overestimated by the DFT computations. Furthermore, it proved impossible to find experimental evidence of the ^{14}N hyperfine coupling predicted theoretically for N2. Although it cannot be ruled out that the latter contribution is not observed due to the large anisotropy of the hyperfine tensor, it is more likely that the DFT computations also overestimate this contribution. Considerable discrepancy between experiment and DFT theoretical predictions has been found for other cobalt-containing complexes and is due to known problems of the current state-of-the-art DFT in predicting EPR parameters of transition-metal complexes.[48−50]

Mechanistic Considerations for Formation of $[Co^{III}(\mathbf{1}^{\bullet})(OAc)_{1,2}](OAc)_{1,0}$. In our previous work, we have shown that the addition of acetic acid to [Co(**1**)] under anaerobic conditions results in the formation of acetate-/acetic acid-ligated [Co(**1**)] complexes ((*R*,*R*)-$[Co^{II}(\mathbf{1})(OAc)_n]^{n-}$ ($n = 1, 2$)).[33] Subsequent addition of oxygen results in, among other things, the formation of the minority species A discussed above. This shows that oxygen plays a key role in the formation of the phenoxyl radical. Furthermore, the coordination of acetate appears to be crucial for the specific formation of the phenoxyl radical $[Co^{III}(\mathbf{1}^{\bullet})(OAc)_{1,2}](OAc)_{1,0}$. This important assertion was proved by the following experiment. Pyridine was added to the precursor complex (*R*,*R*)-$[Co^{II}(\mathbf{1})(OAc)_n]^{n-}$ (i.e., formed by acetic acid addition to the (*R*,*R*)-[Co^{II}(**1**)] precatalyst under a N_2 atmosphere); this results in the formation of mono- and bis-pyridine-ligated [Co(**1**)] (Supporting Information). When molecular oxygen was subsequently exposed to this $[Co^{II}(\mathbf{1})(Py)_{n=1,2}]$ adduct, the superoxo cobalt(III) complex, $[(Py)Co^{III}(\mathbf{1})(O_2^-)]$, was formed and easily identified in the EPR spectrum, while no trace of species B was found (data not shown, Table 1).

The observation of $[Co^{III}(\mathbf{1}^{\bullet})(OAc)_{1,2}](OAc)_{1,0}$ implies that the aerobic oxidation of [Co^{II}(**1**)] in the presence of acetic acid must couple the two-electron, two-proton reduction of oxygen to H_2O_2 (Scheme 2). Although the intermediate superoxocobalt(III) species was not directly observed in

Scheme 2. Schematic Illustration of the Proposed Mechanism for the Formation of $[Co^{III}(1^{\bullet})(OAc)_{1,2}](OAc)_{1,0}$ (Species A) Starting from $[Co^{II}(1)]$

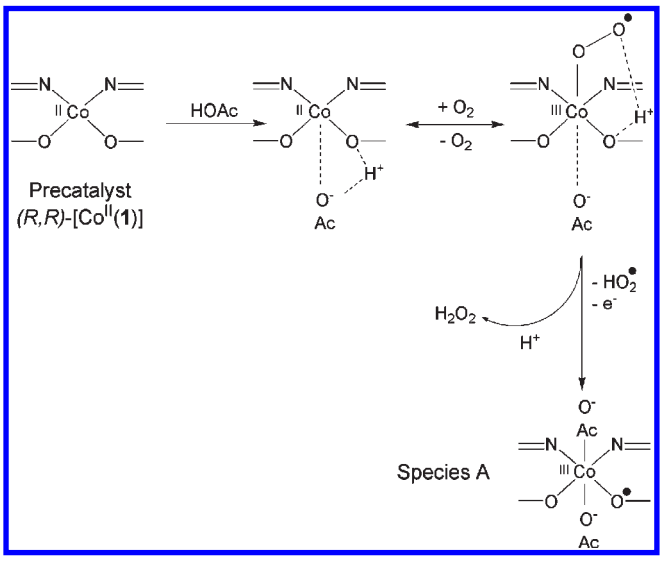

the presence of acetate, its existence is essential to achieving the final oxidized state of the complex (species A). In some ways, this mechanism is reminiscent of the half reaction observed in the fungal enzyme galactose oxidase. In that case, a single copper and modified tyrosine residue couple the two-electron, two-proton oxidation of primary alcohols to the corresponding aldehyde and the two-electron, two proton reduction of dioxygen to hydrogen peroxide.

It should also be mentioned that the formation of species A may be considered to proceed in a manner similar to that described for generating phenoxyl radicals using phenols or quinones in the [Co(salen)] complex, as described previously by Canevali et al.[35] In the first step, the coordination of propenoidic phenols and oxygen by the cobalt−salen complex resulted in the formation of the superoxocobalt(III) center ($[Co^{III}(salen)\ (ROH)(O_2^{-})]$), with subsequent reaction with a second phenol (ROH) leading to the formation of the peroxyl radical ($RO^{\bullet}$), which coordinates to cobalt. It was hypothesized that, in the final step, H^+ loss by the ROH substrate results in the formation of H_2O_2:

$$[Co^{II}(salen)] + ROH + O_2 \leftrightarrow [Co^{III}(salen)(ROH)(O_2^{-})] \quad (3)$$

$$[Co^{III}(salen)(ROH)(O_2^{-})] + ROH \leftrightarrow [Co^{III}(salen)(ROH)(RO^{\bullet})]^{+} + HO_2^{-} \quad (4)$$

$$[Co^{III}(salen)(ROH)(RO^{\bullet})]^{+} + HO_2^{-} \leftrightarrow [Co^{III}(salen)(RO^{-})(RO^{\bullet})] + H_2O_2 \quad (5)$$

However, as stated earlier, the radical in that reported case[35] was based on the ligated $RO^{\bullet}$ substrate and was not ligand derived as for species A.

Conclusions

One of the most successful catalysts for the hydrolytic kinetic resolution of racemic epoxides is based on the chiral cobalt−Schiff base complex [Co(**1**)]. Before use, this precatalyst is first activated by stirring the complex with a weak organic acid under aerobic conditions. Although the precise nature of all the paramagnetic and diamagnetic species formed in the resultant aerobically activated system remains unclear, in this work we have provided a thorough and comprehensive characterization of the identity of one of these paramagnetic species, namely, a coordinated Co^{III} phenoxyl radical, formally assigned as $[Co^{III}(1^{\bullet})(OAc)_{1,2}](OAc)_{1,0}$. The formation of this radical was proposed to occur in the presence of acetic acid by coupling the two-electron, two-proton reduction of molecular oxygen to H_2O_2. Extensive EPR experiments proved that the unpaired electron was localized on the **1** ligand and did not originate from a coordinated axial species (such as a bound radical). This finding was supported by RR and DFT computations. While ligand **1** has been known to stabilize the phenoxyl radicals of $[Cu^{II}(1)]$ and $[Ni^{II}(1)]$, this is the first report of the radical being formed in the [Co(**1**)] system and by nonelectrochemical means. While the phenoxyl $[Co^{III}(1^{\bullet})(OAc)_{1,2}](OAc)_{1,0}$ species represents only a minority part of the entire activated [Co(**1**)] complex, these results offer a unique glimpse into the complexities of the resultant paramagnetic species that can be formed in this important catalytic system.

Acknowledgment. The research was supported by the Fund of Scientific Research—Flanders (FWO; Project G.0312.05N to S.V.D.). E.V. is a research assistant of the FWO. D.M.M. and I.A.F. acknowledge the support of EPSRC (EP/E030122, GR/L80447/01, EP/C528638/1, EP/C53090X/1).

Supporting Information Available: Formation of species A after the addition of formic acid, temperature dependence of the CW-EPR signal of species A, addition of pyridine under anaerobic conditions to the precursor complex, HYSCORE analysis of species B, DFT computations on cobalt-bound phenoxyl radicals, activation of the catalyst with ^{13}C-labeled acetic acid, nitrogen HYSCORE spectra of species A, proton HYSCORE spectra of species A, simulation of the X-band CW-EPR spectrum of species A, including the strongest nitrogen and proton hyperfine interactions as computed by DFT. This material is available free of charge via the Internet at http://pubs.acs.org.